International Journal of Hydrogen Energy 222 (2026) 154311

Contents lists available at ScienceDirect

International Journal of Hydrogen Energy

journal homepage: www.elsevier.com/locate/he

Development and validation of an integrated analog control system for a 30W PEM fuel cell powered by a 100W H_2 generator

Ephrem Ryan Alphonsus [a], Mohammad Omar Abdullah [a,b,*], Ahmed M.A. Haidar [b,c], Abadi Chanik [b,c], Ibrahim Yakub [a,b], Thossaporn Wijakmatee [d], Hideyuki Matsumoto [d]

[a] Department of Chemical Engineering & Energy Sustainability, Faculty of Engineering, Universiti Malaysia Sarawak (UNIMAS), 94300, Kota Samarahan, Sarawak, Malaysia
[b] Hydrogen Production, Techno-economy & Sustainability (HPTeS) Research Group, Faculty of Engineering, Universiti Malaysia Sarawak (UNIMAS), 94300, Kota Samarahan, Sarawak, Malaysia
[c] Department of Electrical and Electronic Engineering, Faculty of Engineering, Universiti Malaysia Sarawak, 94300, Kota Samarahan, Malaysia
[d] Department of Chemical Science and Engineering, Institute of Science Tokyo, 2-12-1, Ookayama Meguro-ku, Tokyo, 152-8550, Japan

ARTICLE INFO

Keywords:
Integrated control
PEM fuel cell
PEM electrolyzer
System integration
Energy management system
Experimental validation

ABSTRACT

This study addresses the need for intelligent management in integrated hydrogen energy systems by designing and validating a cost-effective analog control system for a proton exchange membrane (PEM) fuel cell stack powered by a PEM electrolyzer. The work first characterizes a commercial GL-200 electrolyzer, establishing a baseline hydrogen production rate of 210 ml/min at 185 kPa with an efficiency of 33.7–42.7%. The evaluation of its standard timer-based controller reveals critical limitations: a lack of real-time monitoring and a fixed exhaust cycle that induces voltage fluctuations exceeding 7 V under dynamic load. To overcome these issues, a novel analog controller was developed. The core optimization goal of this controller is to ensure stable and safe operational control of the integrated PEM fuel cell stack under dynamic conditions, with a primary focus on preventing voltage instability through adaptive purge cycle management. This system employs dedicated sensors to continuously monitor stack voltage, temperature, and pressure. Its key innovation is a pressure-triggered exhaust valve activation (at 200 kPa), which replaces the inflexible fixed-timer logic to achieve this goal. This results in significantly more stable and safer operation, maintaining a consistent stack output voltage of 10.5 V. A major advantage is the dramatic reduction in unit cost; the prototype controller is fabricated for under MYR 200, representing an approximately 18-fold reduction compared to the commercial benchmark. While the current prototype requires an external low-voltage power source, this work demonstrates a pivotal step towards viable, intelligent control for small-scale, renewable hydrogen-based power systems.

1. Introduction

Electrolysis offers an efficient and sustainable pathway for green hydrogen production, producing only oxygen as a by-product. Unlike conventional steam methane reforming, which emits CO_2 [1], electrolysis powered by renewables provides a cleaner alternative [2–4]. However, the widespread adoption and scalability of this technology remain hindered by persistent economic and technical barriers, with control systems for dynamic operation under variable power being a key challenge [5,6]

Among available electrolysis technologies, proton exchange membrane (PEM) electrolysis stands out due to its high efficiency, high-purity output, compact design, and operational flexibility at high current densities [7,8]. The use of a solid proton-conducting membrane allows high-pressure operation with low gas permeability, making it ideal for integration with renewable energy sources. Continuous research efforts aim to further enhance these characteristics, with recent reviews highlighting advances in catalyst development, novel proton exchange membranes, and improved gas diffusion layers aimed at increasing efficiency, durability, and cost-effectiveness. However, advanced control strategies are essential to address key operational challenges such as thermal regulation, water management, membrane

* Corresponding author at: Department of Chemical Engineering & Energy Sustainability, Faculty of Engineering, Universiti Malaysia Sarawak (UNIMAS), 94300, Kota Samarahan, Sarawak, Malaysia
E-mail addresses: amomar@unimas.my, amomar13@gmail.com (M.O. Abdullah).

https://doi.org/10.1016/j.ijhydene.2026.154311
Received 13 October 2025; Received in revised form 22 January 2026; Accepted 27 February 2026
Available online 3 March 2026

hydration, process safety and dynamic electrical response under fluctuating power conditions [9]. Bakır and Ağbulut [10] develops a novel arctic puffin optimization based on quasi-opposition-based learning and dynamic fitness-distance balance for more efficient design, operation, and control of PEMFC systems. Qi et al. [11] study proposes a multi-wavy channels flow field design with a stretch factor to achieve progressive flow oscillation for synergistic optimization of mass transfer and water management that integrates a 3D Multiphysics PEMFC model with a neural network-NSGA-II (Non-dominated Sorting Genetic Algorithm II) optimization framework. Similarly, recent work demonstrates the application of advanced metaheuristic algorithms, such as the Improved Coot Optimizer, for optimizing PEMFC operating parameters to stabilize voltage output under varying load conditions, underscoring the critical role of intelligent control.

To address these challenges, most research has focused on sophisticated control and modelling strategies. For instance, advanced control-oriented strategies like cascade internal model control have been developed to manage thermal dynamics under varying loads [12,13]. Concurrently, novel modelling approaches utilizing functions like the g-function combined with self-adaptive differential evolution algorithms offer improved accuracy and numerical stability for control system design. Furthermore, nonlinear control strategies, such as Feedback Linearization-based Adaptive Sliding Mode Controllers, have been proposed for the precise, coordinated management of anode and cathode gas pressures [14].

However, these sophisticated digital and model-based strategies often involve complexity and cost that are prohibitive for small-scale, research-focused, or portable integrated energy systems. This creates a clear and pertinent gap in the literature: a lack of validated, ultra-low-cost, and hardware-reliant analog control solutions where simplicity, reliability, and affordability are paramount. To address this gap, this study aims to develop and validate a novel, low-cost analog control framework for a small-scale, integrated PEM fuel cell system. The core objective is to design, prototype, and test a new fuel cell (FC) controller that prioritizes cost-effectiveness and hardware-based reliability. This controller features integrated real-time monitoring of voltage, temperature, and pressure via analog sensors, offering a significant functional and economic advantage over typical commercial units.

To this end, a compact GL-200 Hydrogen Generator System (100W input, 30W fuel cell) was selected as the experimental platform. Given these control challenges, the scope of this study employs a compact GL-200 Hydrogen Generator System (100W input, 30W fuel cell) to experimentally characterize PEM electrolyzer performance and evaluate control system functionality under realistic operational conditions. The core optimization goal of the developed analog controller is to ensure stable and safe operational control of the integrated PEM fuel cell stack under dynamic conditions, with a primary focus on preventing voltage instability through adaptive purge cycle management. This study aims to fill the gap of establishing an accurate and simple methodology on evaluating the performance of a procurable hydrogen generator in the current market. The study further aims to develop an optimized new FC control framework to address critical gaps in PEM-based electrolysis systems for sustainable hydrogen production. The new FC controller design, fabrication and experimental validation of a novel control system for PEM fuel cells includes features with improved functionality in integrated real-time system monitoring and diagnostics voltage, temperature, and pressure monitoring via analog input, offers significant advantages over typical commercial-supplied controllers. Another significant advantage for the new FC controller compared against the commercially-supply controller is its low-cost and can be customized for any low powered FC.

Currently, the hydrogen generator industry features various range of manufacturers that are competing in the global market. A few manufacturers currently operating in the hydrogen generator industry market are Parker Hannifin, PEAK Scientific, Shandong Saikesaisi Hydrogen Energy, LNI Swissgas, Tianjin Hyvoda Hydrogen Energy Technology. Manufacturers such as LNI Swissgas [15], PEAK Scientific [16], Parker Hannifin [17] and Shandong Saikesaisi [18] provide compact high-purity PEM electrolyzers suitable for laboratory and research applications. These hydrogen generators operate with volume flow rates between 160 mL/min and 500 mL/min, depending on the model selected. Additionally, these units produce ultra-high purity hydrogen, exceeding 99.999% for sensitive applications. Tianjin Hyvoda Hydrogen Energy [19] supplies hydrogen generators designed to meet demands of the petroleum, electronics, medical and chemical energy sectors. This focus on research and specialized industrial applications occurs alongside a significant push for large-scale commercialization, with major industry players like Bosch scaling up PEM electrolyzer production to the gigawatt level, supported by strong global market growth forecasts.

Furthermore, while commercial controllers are essential and effective for many applications, studies show that traditional control methods can have limitations under highly dynamic operating conditions, such as those involving variable renewable inputs [20]. These limitations can relate to handling multiple, simultaneous parameter fluctuations which are critical for efficiency and longevity. Our work therefore focuses on developing a cost-effective analog control solution tailored to address these specific challenges in small-scale, integrated systems, filling a niche where advanced functionality is needed but complex digital controllers may be cost-prohibitive.

The GL-200 employed in this study is positioned as a mid-range, research-grade unit. The comparison focuses on key operational parameters relevant to integrated system design: hydrogen production rate, output pressure, typical efficiency, and intended application scope - the summary of which is provided below for the readers' convenience.

- GL-200 (This Study): 210 ml/min, 185 kPa, 33.7–42.7% efficiency (LHV), research & demonstration systems.
- Typical Lab Generators (e.g., PEAK Scientific): 160-500 ml/min, 100-200 kPa, >99.999% purity, analytical instrumentation.
- High-Pressure/High-Capacity Units (e.g., Nel, H-TEC): >1 L/min, up to 30+ bar, >65% efficiency (LHV), energy storage, refuelling.

Consequently, this study aims to.

(1) Experimentally characterize the overall performance of the GL-200 PEM electrolyzer system under varying operational conditions.
(2) Evaluate the functionality and limitations of its existing timer-based control system in managing dynamic operation.
(3) Design, prototype, and validate a novel analog FC controller.

The key innovation of this controller is the replacement of inflexible timer-based purge logic with a sensor-driven, pressure-triggered valve activation (at 200 kPa), enabling adaptive control based on actual system state. This approach offers a blueprint for radically affordable, intelligent control in small-scale renewable hydrogen systems.

2. Methodology

2.1. Operational principles of hydrogen generator 100 W GL -200 and the incorporation of a new fuel cell controller

The Hydrogen Generator GL – 200 manufactured by Shandong Saikesaisi Hydrogen Energy Co. operates like a typical electrolyzer. It uses deionized water for electrolysis. The system can produce a 99.999% or above purity of hydrogen gas [18]. The schematic diagram of the GL-200 Hydrogen Generator (without fuel cell) is given in Supplementary Material, Fig. A1. Fig. A2 shows the full assembly of Hydrogen Generator with a 30 W Fuel Cell. Fig. A3 is the close-up look of the Fuel Cell assembly (before introducing new FC controller). The operation parameters of the hydrogen generator and the fuel cell are given in Supplementary Material, Table A1 and Table A2, respectively. While the

overall system exhibits good performance, however, the control subsystem exhibits a limitation in temperature and pressure monitoring functionality. Specifically, the FC controller is preset to activate the exhaust valve at 5 s and terminate the output supply of the FC at 10 s. Subsequently, the operational sequence repeats itself.

2.1.1. New fuel cell controller design

In the present study, a new FC controller assembly is thus designed and built. Therefore, the new overall system can be drawn up schematically as in Fig. 1(a). The new FC controller design specifically identified as: (Automated Voltage-Temperature Monitoring and Pressure-Based Valve Control System using Analog Voltage Input) consists of an Arduino Uno, Liquid Crystal Display (LCD), voltage sensor, temperature sensor, pressure transducer and an analog pressure gauge, Fig. 1(b) and (c) respectively. Fig. 2 is the flowchart of the new FC controller. It describes the process flow of the new FC controller. See Table 1 for the detailed component list and specifications.

The schematic diagram, Fig. 1(b) represents a new smart hydrogen FC management system integrated with voltage, temperature and pressure monitoring, exhaust valve control-regulation and display function. The system begins with hydrogen input into the FC. The voltage sensor will monitor the voltage output of the FC. If the voltage output is below 8.4 V, the Green Indicator will not be activated. The 8.4 V FC output is the minimum safe-operating voltage. If the output is lower, the FC needs to be inspected for malfunction. The temperature monitoring system will measure the current temperature of the FC. If the temperature of the FC is above or equal to 40 °C which is approximately 80% of the optimal temperature, a Red LED will be activated to notify the operator for the increase of temperature. The optimal commercial temperature of the FC is below 55 °C. For pressure monitoring, if the hydrogen pressure exceeds the set threshold of 200 kPa, which is 50% of the system's operational pressure, the controller will send a signal to activate the exhaust valve. The exhaust valve, once activated, will allow the excess hydrogen to exit safely. This will ensure that pressure levels within the system are safe and will prevent damage to the whole system. The new FC controller also incorporates an LCD Display module that provides operational data on all the monitored parameters. The display provides voltage output and temperature of the FC, pressure inside the system and the valve condition i.e whether the exhaust valve is open or closed.

2.2. Mathematical governing equations

2.2.1. Hydrogen production water electrolysis

If voltage greater than 1.23V is applied to the cell, the necessary Gibbs free energy ($\Delta G^0_{298} = 237\ kJ/mol$) is supplied and the water is split with the integration of thermal energy from the environment [8, 21]. The cathode (negative terminal) produces hydrogen, while the anode (positive terminal) produces oxygen according to the following reactions:

$$\text{Anode}: H_2O \rightarrow \frac{1}{2}O_2 + 2e^- + 2H^+ \tag{1}$$

$$\text{Cathode}: 2H^+ + 2e^- \rightarrow H_2 \tag{2}$$

$$\text{Sum}: H_2O \rightarrow \frac{1}{2}O_2 + H_2 \left(\Delta H^0_{298} = 286 \frac{kJ}{mol}\right) \tag{3}$$

The cell's efficiency, $\eta_{cell,LHV}$ Eq. (4), can be determined by [8],

$$\eta_{cell,LHV} = \frac{1.23V}{E_{cell}} \tag{4}$$

where,

E_{cell} is the cell voltage.

Overall reactions of the electrolysis cell (Eq. (3)) provided the required stoichiometric coefficients for the products and reactant used in Eq. (5). The sign convention is positive for products and negative for reactants with analogous definitions for ΔB, ΔC and ΔD. Data for the constants A, B, C and D are thermodynamic properties and are reproduced in Table 2.

$$\Delta A \rightarrow A_{H_2} + \frac{1}{2}A_{O_2} - A_{H_2O} \tag{5}$$

The model uses the specific heat capacity of water and gases in the ideal state to determine the standard Gibbs free energy of reaction, ΔG^o, i.e., Eq. (6),

$$\Delta G^o = RT\left[\frac{\Delta G^o_0 - \Delta H^o_0}{RT_0} + \frac{\Delta H^o_0}{RT} + \frac{1}{T}\int_{T_0}^{T}\frac{\Delta C^o_p}{R}dT - \int_{T_0}^{T}\frac{\Delta C^o_p}{R}\frac{dT}{T}\right] \tag{6}$$

where ΔH^o_0 and ΔG^o_0 are the standard enthalpy and Gibbs energy of formation of liquid water, respectively, at reference temperature T_0. The integrals of Eq. (6) consider the temperature dependency of the heat capacities of the products and reactants and are reduced to Eq. (7) and Eq. (8),

$$\int_{T_0}^{T}\Delta C^o_p dT = (\Delta A)T_0(\tau - 1) + \frac{\Delta B}{2}T_0^2(\tau^2 - 1) + \frac{\Delta C}{3}T_0^3(\tau^3 - 1) + \frac{\Delta D}{T_0}\left(\frac{\tau - 1}{\tau}\right) \tag{7}$$

$$\int_{T_0}^{T}\frac{\Delta C^o_p}{R}\frac{dT}{T} = \Delta A ln\tau + \left[\Delta BT_0 + \left(\Delta CT_0^2 + \frac{\Delta D}{\tau^2 T_0^2}\right)\left(\frac{\tau + 1}{2}\right)\right](\tau - 1) \tag{8}$$

T – is reaction temperature (K),

T_0 – reference temperature (298 K)

R – universal gas constant (8.314 J mol^{-1} K^{-1})

tau, τ – defined as $\tau \equiv T/T_0$

The simplified version of Gibbs Energy Equation by Anwar et al. [22] and Chisholm and Cronin [23] can be observed in Eq. (9). The minimum requirement of water decomposition voltage as a function of temperature and pressure is defined by Gibbs free energy [22].

$$\Delta G = \Delta H - T\Delta S \tag{9}$$

ΔG = Gibbs free energy of water formation, kJ/mol

ΔH = Enthalpy charge of water formation,

$T\Delta S$ = Entropy changes of water formation (multiplied by temperature, T).

The equilibrium cell voltage *Eeq* is determined by the Gibbs free energy as shown in Eq. (10).

$$\Delta G = -nFEeq \tag{10}$$

Where,

n - number of moles of electron transferred,

F - Faraday's constant and

Eeq - the equilibrium voltage.

Considering water dissociation, n, the number of moles of electron transfer in the reaction is 2e-, and the value of F is 96,485 C/mol. At the standard temperature of (25^0C) and pressure (1 atm) condition, ΔG = 274.2 kJ/mol and Eeq = 1.23V and the current efficiency is 100% [22]. At standard temperature and pressure (STP, 25 °C, 1atm) Gibbs free energy of formation is defined as the point of zero energy and is used to calculate the change in energy of a system. The reversible (i.e., the minimum) voltage required to electrolyze water into hydrogen and oxygen is determined can also be determined as, Eq. (11).

$$E_o = -\frac{\Delta G^o}{zF} \tag{11}$$

E_o – the theoretical minimum reversible voltage of a cell

z – the number of electrons (2) taking part in the reaction

Actual voltage (V_{cell}) required to decompose water at any significant

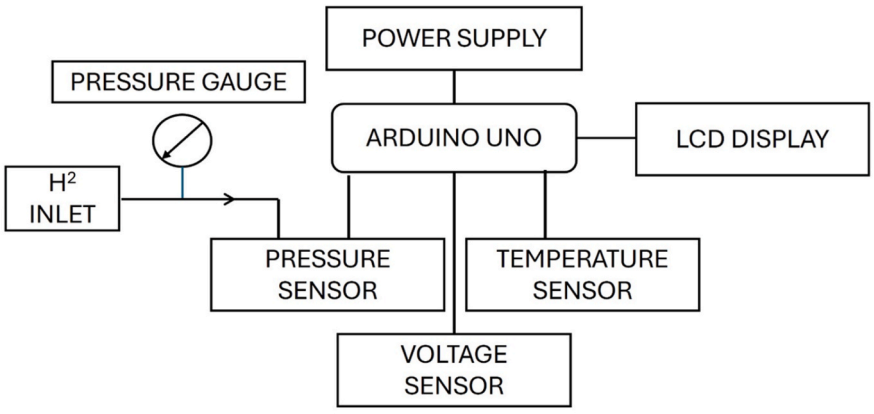

(a)

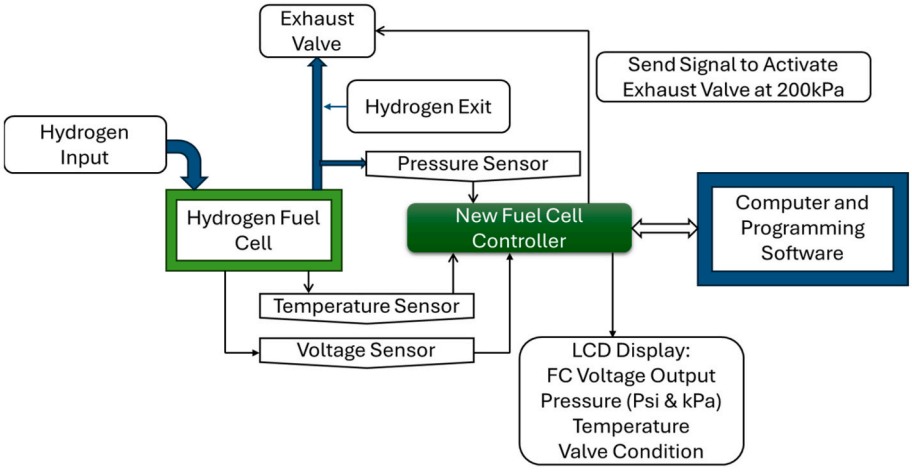

(b)

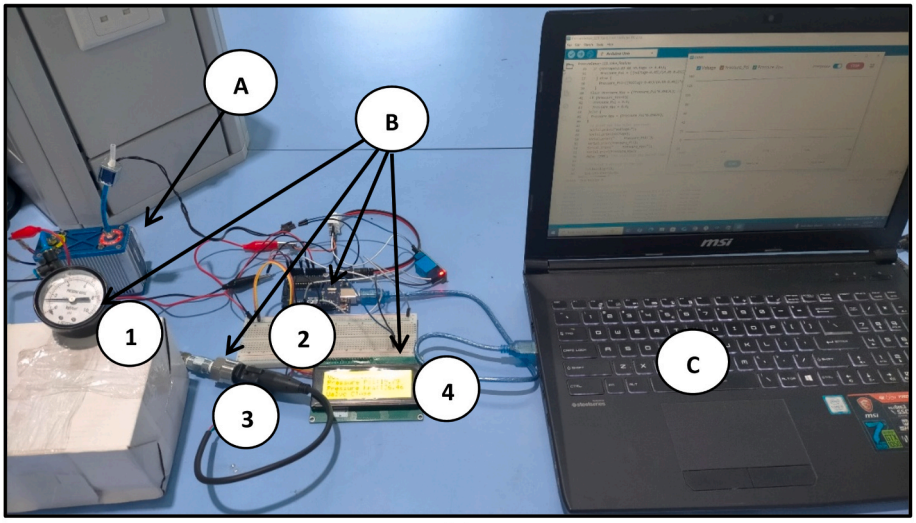

(c)

Fig. 1. New FC Controller (a) Schematic Diagram of Automated Voltage-Temperature Monitoring and Pressure-Based Valve Control System using Analog Input (b) Schematic Diagram of the New Overall System: Automated Voltage-Temperature Monitoring and Pressure-Based Valve Control System using Analog Input (c) New FC Controller Assembly (B and C): (A) Fuel cell attached with Voltage-Temperature Sensor, (B)-(1) Pressure gauge (2) Arduino Uno (3) Pressure Transducer Transmitter Sensor (4) LCD Screen and (C) Laptop and Programmer.

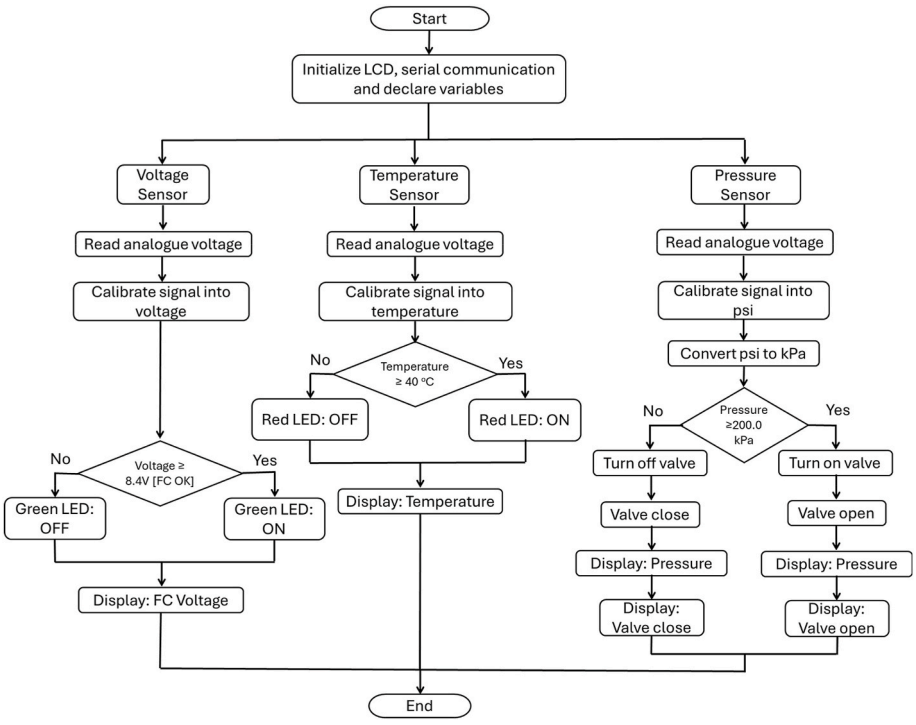

Fig. 2. Flowchart of an Automated Voltage-Temperature Monitoring and Pressure-Based Valve Control System using Analog Voltage Input.

Table 1
New fuel cell controller components of automated voltage-temperature monitoring and pressure-based valve control system using analog input.

Components	Specifications
Controller	Arduino Uno
Analog Pressure Gauge	Unijin Pressure Gauge 150 psi
LCD	Soldered Serial 12C LCD 16x2 20x4 IIC Twi Spi for Arduino Green/Blue 1602 2004
Pressure Sensor	SPB DC5V 1/8NPT 6
Temperature Sensor	DS18B20
Voltage Sensor	25V

Table 2
Constants for heat capacities of gases in ideal state and liquid water. (Harrison and Levene, 2008).

	A	B	C	D
H_2	3.249	$0.422x10^{-3}$	0	$0.083x10^{5}$
O_2	3.639	$0.506x10^{-3}$	0	$-0.227x10^{5}$
H_2O	8.712	$1.25x10^{-3}$	$-0.18x10^{-6}$	0

rate will require V_{cell} be greater than E_o. The difference between the voltages is known as overpotential, polarization or simply losses [8].

Nernst potential (V_n) of Eq. (12).

$$V_n = E_o + \frac{RT}{2F} ln\left(\frac{P_{H_2} P_{O_2}^{1/2}}{P_{H_2O}}\right) \tag{12}$$

P_{H_2}, P_{O_2} and P_{H_2O} represent the partial pressures of hydrogen, oxygen and water.

Partial pressure of water in Eq. (13).

$$P_{H_2O} = 610.78\ exp\left[\frac{T_c}{T_c + 238.3}(17.2694)\right] \tag{13}$$

T_c – temperature into the stack in ^{o}C.

The partial pressure of hydrogen and oxygen, can be determined using measurements from the stack cathode and anode, Eq. (14) and Eq. (15).

$$P_{H_2} = P_C - P_{H_2O} \tag{14}$$

$$P_{O_2} = P_A - P_{H_2O} \tag{15}$$

P_C– experimental pressure (atm) of the cathode
P_A- experimental pressure (atm) of the anode

2.2.2. *Ohmic losses of electrolysis*

Ohmic losses occur because of resistance to the flow of ions in the solid electrolyte and resistance to flow of electrons through the electrode materials. The ohmic overpotential, η_o of Eq. (16) [8],

$$\eta_o = \frac{\varphi}{\sigma} i \tag{16}$$

where,
i - function of the stack current density,
φ - the membrane thickness, and
σ - the conductivity of the stake.

2.2.3. *Electrolyzer efficiency*

Electrolyzer efficiency η_{el} is the efficiency of the hydrolysis reaction at constant temperature and pressure [24]. The electrolyzer efficiency Eq. (17),

$$\eta_{el} = \eta_i \eta_v \tag{17}$$

where,
η_v - voltage efficiency and
η_i - current efficiency.

The current efficiency Eq. (18), also known as Faraday efficiency, can be expressed as:

$$\eta_i = 96.5 e^{\frac{0.09}{I} - \frac{75.5}{I^2}} \tag{18}$$

where I is the stack current of the electrolyzer.

Voltage efficiency Eq. (19), is the ratio between the theoretical

decomposition voltage of water and the actual decomposition voltage, which can be expressed as:

$$\eta_v = (U_{tn} / U_{el})^*100\% \quad (19)$$

where,

U_{tn} - theoretical decomposition voltage, which is 1.482 V and

U_{el} - actual decomposition voltage.

The input power of the electrolyzer P_{el} is related to the electrolyzer current I as follows

$$P_{el} = U_{el} I \quad (20)$$

2.2.4. Fuel cell

2.2.4.1. Fuel cell Governing equation. Hydrogen can react with oxygen to release electric energy and heat according to the inverse process of the electrolysis of water. The FCs consist of two electrodes where the electrochemical reactions take place, an electrolyte ensuring the transfer of ions and a membrane separating the cathode portion of the anodic part of the cell [25].

$$\text{Anode} : 2H_2 \rightarrow 4e + 4H^+ \quad (21)$$

$$\text{Cathode} : O_2 + 4e + 4H^+ \rightarrow 2H_2O + heat \quad (22)$$

Yunez-Cano et al. [26] derived equations on proton exchange membrane fuel cell (PEMFC) on stack efficiency (η_{FC}), Eq. (23).

$$\eta_{FC} = \varepsilon_{FC} / E_{NH_c} \quad (23)$$

which ε_{FC} is the produced energy by FC, Eq. (24).

$$\varepsilon_{FC} = I_{FC} V_{FC} t \quad (24)$$

where,

t operating time,

I_{FC} current produced and

V_{FC} total potential produced of the stack.

The efficiency (η_{FC} and η_{PEME}) depends on the density power of the monocell (W/cm^2) and their respective extrapolation equations. The size parameter (F_{size}), Eq. (25).

$$F_{size} = Ae.N_{stack} \quad (25)$$

where,

Ae geometric area of the electrode and

N_{stack} number of cells in the stack.

The maximum power from the stack, P_{m_stack} Eq. (26).

$$P_{m\_stack} = (P_{m\_cell})(F_{size}) \quad (26)$$

where,

P_{m_cell} monocell maximum power and

F_{size} the size parameter.

2.2.4.2. Fuel cell hydrogen consumption. The hydrogen flow and oxygen consumed by a FC is directly proportional to the current delivered. Energy efficiency varies between 65% when the current density is zero and 34% when the voltage limits at 0.5V [25].

$$F_{O_2} = \frac{N \times I_P}{n \times F \times \eta_F} \text{ and } F_{H_2} = \frac{N \times I_P}{n \times F \times \eta_F} \quad (27)$$

F_{H_2} is the hydrogen flow consumed by the fuel cell (mol/s),

F_{O_2} is oxygen flow consumed by the FC (mol/s),

N is the number of cells in the FC,

η_F is Faraday efficiency, this efficiency is generally very close to 1,

n is the number of electron exchange (n = 2 for H_2, n = 4 for O_2).

2.3. Sensor calibration equations

Arduino Uno uses a 10-bit Analog to Digital Converter (ADC), which converts analog input voltages into digital values in the range of 0 to 1023, with 0 representing 0V and 1023 representing 5.0V. The information from Table 3 for the pressure transducer will be applied for Eq. (28).

Sensor voltage V_s, can be estimated as in Eq. (28).

$$V_s = \frac{adc_{raw} \times 5}{adc_{resolution}} \quad (28)$$

where,

$adc_{resolution}$ Analog to Digital Converter resolution is 1023 and

adc_{raw} – raw data (ADC) read from pressure transducer.

The calibrated pressure (Eq. (29)) in psi, p_{psi}

$$p_{psi} = \frac{V_s - V_{min}}{V_{max} - V_{min}} \times p_{psi_{max}} \quad (29)$$

where,

V_{min} minimum voltage of sensor reading,

V_{max} maximum voltage of sensor reading and

$p_{psi_{max}}$ maximum sensor reading in psi.

To convert the pressure value from psi into kPa, p_{kpa}, Eq. (30).

$$p_{kpa} = 6.89476 \times p_{psi} \quad (30)$$

2.4. Energy management

The energy balance system can be described as, Eq. (31).

$$E_{in} - E_{out} = \Delta E \quad (31)$$

where,

E_{in} energy in,

E_{out} energy out and

ΔE change of energy.

By applying Eq. (31) into our system, we can derive Eq. (32).

$$E_{in} = E_{out} + \Delta E \quad (32)$$

Convert energy into power and we can come up with Eq. (33).

$$P_{in} = P_{out} + \Delta P \quad (33)$$

where,

P_{in} power in,

P_{out} power out and

ΔP change of power.

Derived Eq. (33) into our system, which $(P_{out} + \Delta P)$ can be substituted into, power for electrolysis and power of the system to activate the hydrogen generator, Eq. (34).

$$P_{in} = P_{el} + P_{hgen:operate} \quad (34)$$

where,

$P_{hgen:operate}$ minimum power needed for hydrogen generator to operate.

Table 3
Technical information of pressure transducer transmitter sensor.

Sensor	SPB DC5V 1/8NPT 6
Specifications	Oil Air Water
Input	0 – 100 psi
Output	0.5 V ~4.5 V linear voltage output. 0 psi outputs, 0.5V, 50 psi outputs 2.5V, 100 psi outputs 4.5V.
Accuracy	Within 2% of reading (full scale)

2.5. Mathematical equations derived from experimental results

To calculate the overall efficiency of hydrogen generator, the volume flowrate $\dot{V}$, is first determined by Eq. (35).

$$\dot{V} = \frac{V}{t} \tag{35}$$

where,

V volume in L and t time.

Molar volume, can be determined from Eq. 36

$$V_m = V_m^o \times \frac{T}{T^o} \tag{36}$$

where,

Standard conditions, temperature, T^o (1 atm, 273.15K), molar volume of an ideal gas is $V_m^o = 22.414$ l/mol and T is lab temperature.

The molar flow rate, $\dot{n}$, $\left(\frac{mol}{s}\right)$ Eq. (37).

$$\dot{n} = \frac{\dot{V}}{V_m} \tag{37}$$

Using Gibbs free energy of water electrolysis, which is 237 kJ/mol for hydrogen production, P_{ideal} can determined, Eq. (38).

$$P_{ideal} = \dot{n} \times \Delta G \tag{38}$$

The actual power requirement of the electrolysis depends on the efficiency (η_{el}), Eq. (49) Eq. (39).

$$\eta_{el} = \frac{P_{ideal}}{P_{actual}} \tag{39}$$

$$P_{actual} = \frac{P_{ideal}}{\eta_{el}} \tag{40}$$

Using this value, we can determine the minimum power that can be used to operate the hydrogen generator by taking account of the actual power needed for electrolysis and energy losses [8] when the efficiency is at the lowest, Eq. (41) and Eq. (42) can be derived.

$$P_{in} = P_{min} + P_{\eta=55\%} \tag{41}$$

$$P_{min} = P_{in} - P_{\eta=55\%} \tag{42}$$

where,

P_{min} power needed to activate the system,

P_{in} operating power input for the whole system and

$P_{\eta\ =\ 55\%}$; power needed for electrolysis at 55% efficiency.

Using power at 84% efficiency, we can determine the minimum power needed for the hydrogen generator to operate, Eq. (43).

$$P_{hgen:operate} = P_{\eta=84\%} + P_{min} \tag{43}$$

where,

$P_{\eta=84\%}$ actual power at 84% efficiency.

Apply Eq. (43) for experimental data in .Section 3.1.

$$P = V_{exp} I \tag{44}$$

where,

V_{exp} voltage from FC experimental data and

$I = 3.6$ A taken from Table A2.

2.6. Integrated system modeling framework

A detailed system-level mathematical model was developed to provide a rigorous foundation for this study. This model, comprising interrelated equations for electrochemical kinetics, thermodynamics, mass transport, and energy balance, is not merely background theory but serves as the cornerstone for analysis and design.

This framework fulfils three critical and distinct roles.

1. Establishing a Scientific Baseline for Diagnosis: The complete model encapsulates the nominal, steady-state operation of the integrated PEM electrolyzer and fuel cell system. By defining the expected relationships between input power, hydrogen production, stack pressure, and output voltage, it creates a performance benchmark. This benchmark was essential for Objectives 1 & 2, allowing us to characterize the GL-200 system's baseline efficiency and to diagnostically identify the commercial controller's failure to maintain these modeled relationships under dynamic loads, leading to voltage instability.
2. Informing the Empirical Control Strategy: Analysis of the model reveals that stack pressure is a highly effective integrative state variable. Pressure dynamics directly reflect the balance between the electrolyzer's gas production and the fuel cell's consumption, integrating effects of temperature and flow rates. This theoretical insight directly justified the core innovation of our controller: selecting a pressure threshold (200 kPa) as a simple, measurable, and cost-effective proxy for overall system state. Therefore, the pressure-triggered strategy is not an arbitrary choice but an empirical rule logically extracted from and validated by the broader system understanding provided by the full model.
3. Enabling a "Digital Twin" for Future Advancement: The full equation set constitutes a "digital twin" of the physical experimental platform. While the current prototype implements a single-input, single-output control for maximum reliability and minimal cost, this comprehensive model provides the exact mathematical framework required for future research. It enables the direct implementation and testing of sophisticated control strategies—such as Model Predictive Control (MPC) or neural network-based optimizers—on this hardware without requiring new fundamental modeling. Thus, this work provides both an immediately deployable solution and a clear, ready-to-use pathway for next-generation research on advanced control algorithms for small-scale integrated energy systems.

3. Results and discussions

In this section, the results are presented into three main sections for clarity and comprehensive interpretation. In Section 3.1 will focus on the performance of the hydrogen generator. Section 3.2 examines the FC performance with and without the commercial FC controller and Section 3.3 will describe the performance of the newly developed FC controller.

3.1. Hydrogen generator GL-200 performance

The first control experiment that was conducted on the hydrogen generator was investigating the volume flowrate of an electrolyzer as a function of time. The x-axis describes the time (minutes) ranging from 0 min to 60 min, while the y-axis represents the volume flowrate (ml/min). Three experimental replicates are shown in Fig. 3: Test 1 (blue line), Test 2 (orange line) and Test 3 (green line).

The results showed that the hydrogen generator has a stable volume flowrate. The constant output of 210 ml/min was recorded for all three experiments throughout the duration of 60 min. This consistency represents that the hydrogen generator maintains a steady-state operational condition. There were no fluctuations or changes in the volume flowrate over time.

It shows that the hydrogen generator can mitigate any external disturbances such as temperature, pressure variations or power fluctuations. The consistent volume flowrate is contributed by the inbuilt control system [18].

From the result on Fig. 3, we can find the minimum amount of power to operate the hydrogen generator. Lab temperature was $T = 28$ °C

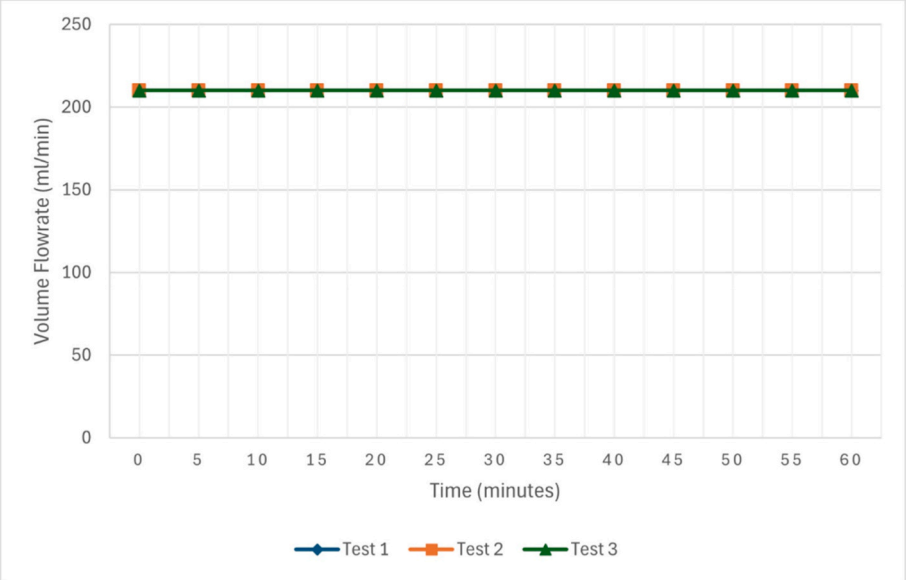

Fig. 3. Volume flowrate of hydrogen generator vs time.

(301.15K) and P_{ideal} can be determined as $P_{ideal} = 33.654\ W$.

From previous studies done by Dawood et al. [7] (efficiency range 67 – 84%) and Zainal et al. [27] (efficiency range 55-70%) the range of efficiency can be stated from 55% to 84%. Using these values, for an efficiency of $\eta = 0.55$, $P_{actual} = 61.19\ W$ and for an efficiency of $\eta = 0.84$, $P_{actual} = 40.06\ W$.

It is known that the power to operate the whole system is given by the manufacturer, which is less than 100 W. Using this value, we can determine the minimum value of power that can be used to operate the hydrogen generator by taking account of the actual power needed for electrolysis and energy losses [8] when the efficiency is at the lowest. It describes that for worst-case scenario, the power exceeds the manufacturer's available power, the hydrogen generator will not be able to operate at the desired output without an energy buffer for it to maintain a safe-stable continuous operation.

At 55% efficiency, the power needed for electrolysis is 61.19 W. By subtracting 61.19 W from the P_{in} =100W, we will get a value of 38.81 W. This is the minimum power needed to operate the hydrogen generator not including for the electrolysis and energy losses.

By using the value of $P_{min} = 38.81$ W, then we can determine the minimum power to operate the whole system including the power needed for electrolysis. By taking the power at 84% efficiency, which is 40.06 W, we can finally determine the minimum power needed for the hydrogen generator to operate. Based on the calculations, we can estimate that the range of power needed to operate the hydrogen generator is between 78.87 W and 100W respectively. Using these values, we can estimate the range of the overall hydrogen generator efficiency, which is $\frac{P_{ideal}}{100W} = 33.7\%$ and $\frac{P_{ideal}}{78.87W} = 42.7\%$. Table 4 provides a performance summary of Hydrogen Generator GL-200.

Fig. 4 presents the time taken to fully discharge hydrogen gas from hydrogen generator immediately after the system is switched off. The x-axis represents time (seconds) and the y-axis represents the output voltage in DC. To establish this outcome, the hydrogen output from the hydrogen generator was connected to a 30W FC and controller. Using the output from the FC, three experimental runs are plotted, namely Test 1(blue line), Test 2 (orange line) and Test 3 (green line) respectively.

From a technical overview, the initial behaviour of all the three experiments commenced at an output of approximately 12 V. This is indicative of the hydrogen generator operating at a stable output (Fig. 3). Across all three tests, sudden voltage drops are observed, which showed the hydrogen discharge process. These voltage drops were indicative of the reduction of hydrogen output since the hydrogen generator was switched off. For Test 1, a full discharge of hydrogen from the system was around 40 s. For Test 2 and Test 3, the full discharge was 59 s and 89 s, respectively. Comparing the outcome of all tests, Test 3 demonstrated prolonged stability while on contrary, Test 1 was the shortest in sustaining discharge.

Overall, Fig. 4 demonstrates the comparative stability of hydrogen discharge across three control experiments. The results indicate that Test 3 sustained hydrogen release for the longest time, which is 89 s whereas Test 1 showed the shortest. This showed significant variability in the hydrogen generator hydrogen output even though the output is constant at 210 ml/min. It may be attributed to change of pressure within the system during the consumption of hydrogen in the FC.

Table 4
Summary of hydrogen generator GL-200 performance.

Performance	Value
Mean Volume Flowrate in 60 min	210 ml/min
Minimum power required to operate hydrogen generator	78.87 W
Maximum power required to operate hydrogen generator	100 W
P_{ideal}	33.654 W
Minimum hydrogen generator efficiency, $\frac{P_{ideal}}{100W}$	33.7%
Maximum hydrogen generator efficiency, $\frac{P_{ideal}}{78.87W}$	42.7%

3.2. Characteristics and performance of 30 watts fuel cell with commercial controller

In this section we will discuss the control experiments that have been conducted on a 30 W FC. The control experiments are divided into two groups which are.

i. FC output with and without FC controller (commercial controller) and
ii. FC connected with New-Analog-Designed FC controller

3.2.1. Fuel cell characterization and performance testing

Fig. 5(a) and (b) presents the results of control experiments examining the voltage output behaviour of a FC (Fig. 5(a) without and Fig. 5 (b) with commercial controller) over time. In Fig. 5(a) the x-axis represents time (minutes), while the y-axis indicates the output voltage (V

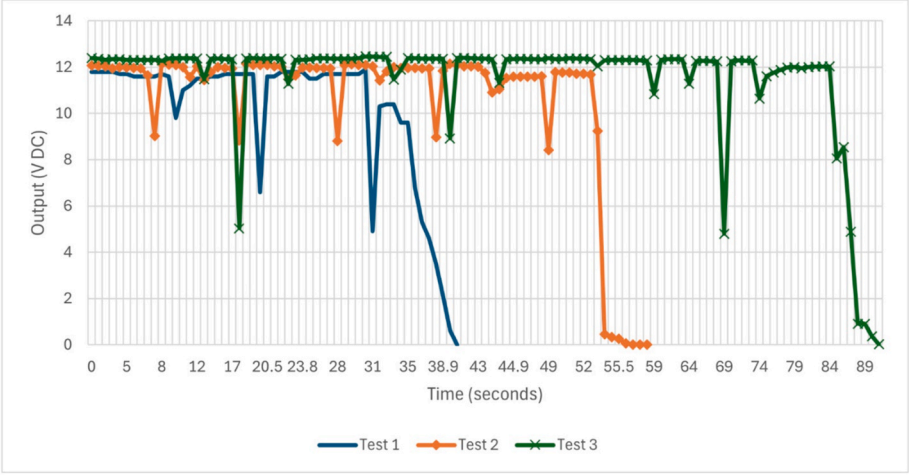

Fig. 4. Time taken to discharge hydrogen from hydrogen generator after switch off.

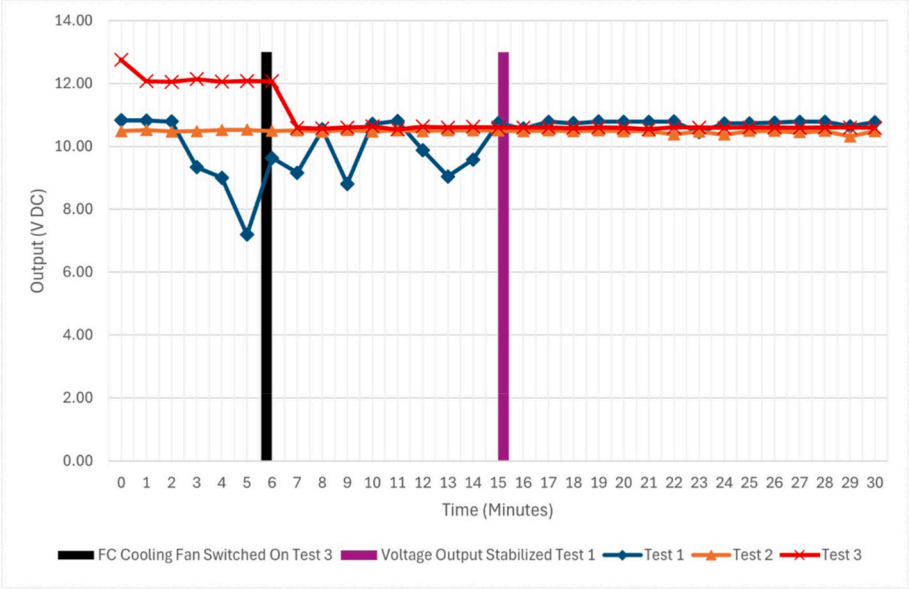

(a)

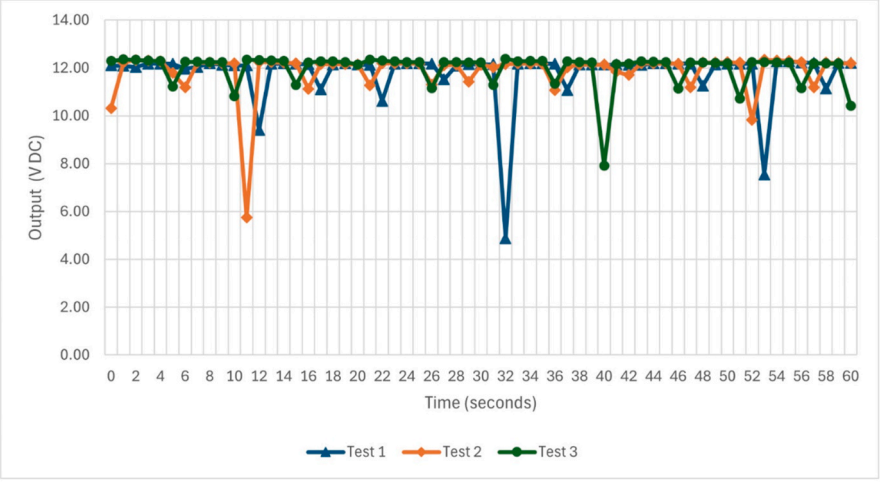

(b)

Fig. 5. Voltage output of (a) fuel cell without controller vs time (b) fuel cell connected with controller (commercial) vs time.

DC). In both control experiments of the FC output voltage (without and with commercial controller), three different tests to determine the voltage output were performed for comparative assessment: Test 1, Test 2 and Test 3.

In Fig. 5(a), a black vertical line at the 5-min mark denotes the activation of the FC cooling fan during Test 3, whereas the purple vertical line at the 15-min marks the point at which Test 1(blue line) voltage stabilization is achieved. Assessing the curves for Test 1, initially in the early minutes of between 0-min to 15-min, Test 1 exhibits voltage fluctuations between 7 V and 11 V. This excessive fluctuation was caused by the initial start-up of the hydrogen generator. It could be the product of increasing pressure from the output of the hydrogen generator. Another possible cause of the excessive fluctuations could be the time taken for the FC reaching stability in consuming the hydrogen, since for Test 1 the system was just activated for control-testing. In reference to the operation manual, there was no information given by the manufacturer on fluctuation of the FC output during startup or at the early minutes of FC output. Subsequently, the voltage output slowly recovers and stabilizes around 10.5 V after the 15-min mark. Test 2 (orange line) shows the most stable profile throughout the duration of 30 min, maintaining a constant voltage out of 10.5 V similarly to Test 1. For Test 3(red line), the voltage outputs begin higher than Test 1 and Test 2, which was reaching 13 V. The reason behind the high voltage value was the FC cooling fan was not activated. An immediate decrease was seen after 6 min, coinciding with the cooling fan being activated during the 5-min and 6-min. Soon after, the voltage remained steady at around 10.5 V like the outputs of Test 1 and Test 2.

Fig. 5(b) shows that the voltage output of three independent test when FC is connected to the commercial FC controller: Test 1(blue line), Test 2(orange line) and Test 3(green line). Analyzing all tests for the FC, the data shows voltage fluctuations between 4.88 V and 12.08 V. The fluctuations are caused by the activation of purging valve and intermittent switching On-Off at the FC. The intervals repeat every 5 s and 10 s. Voltage drop can be observed every time the purging valve is activated at the 5th seconds, and FC will switch off at 10 s intervals and immediately switch back on again. This setting was already embedded inside the FC controller. A small-time delay of approximately 0.3 s was observed in the switching on and off the FC. Voltage drops of up to 7.2 V DC can be observed during the On-Off switching of the FC and another similar voltage drop of up to 0.75 V at the activation of the purging valve were recorded.

In comparison between FC with and without the FC controller, the results showed that the commercial FC controller has a significant impact on the output voltage. An increase of 1.25V can be achieved, if we compare the difference output of FC without controller 10.83V (highest value in between all tests Fig. 5(a)) against the 12.08V commercial FC controller (maximum output in Fig. 5(b)). But on the other hand, a constant fluctuation of voltage does give a negative on the increase. The intermittent switching on and off at every 10 s does not give any benefit to the FC at all. On the contrary, the persistent voltage fluctuations can also accelerate degradation and shorten the lifespan of small devices that are connected to the FC [28,29]. The significant voltage fluctuations observed with the timer-based controller are indicative of mass transport limitations due to ineffective water management. Similar to studies on PEMFC undershoot behavior, these fluctuations likely stem from reactant starvation in the catalyst layer caused by liquid water blockage. Our pressure-triggered purge directly mitigates this by using stack pressure as an integrative variable; an increase toward the 200 kPa threshold signals water/gas accumulation and triggers an adaptive purge, thereby maintaining clear reactant pathways.

3.2.2. Fuel cell efficiency

Using the data in Fig. 5(a) and Table A2, we can calculate the FC efficiency through experimental value. Based on Table A2, the stack efficiency for the FC is stated as 40% at full power. The current is 3.6 A. Using the highest voltage value of 12.08 V and the stable voltage value from each independent tests: for evaluating consistency and stability between Test 1, Test 2 or Test 3, which is 10.5 V, we can determine the maximum power output and the stable power output of the fuel.

The maximum power output is 43.49 W and the stable power output is 37.8 W respectively. The data shows that the difference between the rated power output of 30 W against the experimental value is significant. The reason behind the different values compared with the stated data in the manufacturer operational manual is that the optimal and safest power rating that the FC can generate was selected, even though in Table A2 the manufacturer stated at full power. Furthermore, the commercial FC controller will shut down the FC if it's drawing too much power [18]. The maximum power when the commercial FC controller shuts down the FC is not rated. Referring to a previous study by Valverde et al. [30], the authors stated that manufacturers gave a power rating of 1.5 kW but experimental data showed that the tested power rating was 1813 W, 21% higher than the rated power. The reason was the rated power was only limited to voltage [30] to safeguard the FC from cell damage. The authors' result is related to our experimental data. For our control test, comparing the manufacturer value against the experimental value, the difference is 43.82%.

Using Lower Heating Value (LHV) = 120 MJ/kg and Higher Heating Value (HHV) = 141.90 MJ/kg [31], molar volume of hydrogen at STP (Standard Temperature Pressure) = 22.4 L/mol, molar mass of hydrogen = 2.016 g/mol and flow rate of 210 ml/min we can calculate, the energy input per minute which resulted to 2268 J/min for LHV and 2683.8 J/min for HHV. Employing the FC power rating (manufacturer data) = 30 W. The energy output per minute will be 1800 J/min. Using Equation (23), the efficiency of FC, η_{fc} are 79.37% for HLV and 67.07% for LLV. We can summarize the FC efficiency is between 67% and 79%, if both HLV and LLV were implemented. The FC has better efficiency value, if LHV is used. By comparing the efficiency between LHV and HHV value there is significant difference of around 12%.

3.2.3. Fuel cell voltage efficiency

Applying the result of FC output as 12.08 V when cooling fan is not activated which are assembled into a 14-cells in series, the resultant voltage per/cell is 0.8629V. The voltage efficiency can be calculated by dividing the value with the 1.23 V, Gibbs free energy [8], the η_v is 70.15%. The result indicates that the voltage losses (ohmic losses) account for a significant reduction from the ideal efficiency. The low per-cell voltage suggests that there is room for optimization in terms of reducing losses.

3.2.4. Influence of temperature and pressure on Fuel Cell Performance

Fig. 6(1a) and (2b) illustrate the temporal variation of temperature and pressure towards the FC performance without commercial FC controller. Fig. 6(1a) and (2b) were concurrently tested. Fig. 6(1b) shows the temperature for FC connected to the commercial FC controller vs time.

Fig. 6(1a) demonstrates FC temperature vs time (without the integration of a commercial controller) across three independent tests: Test 1(blue line), Test 2(orange line) and Test 3(dark green line). Test 1, the ambient temperature is stable at around 29.6 °C. The FC temperature starts at around 30.3 °C and stabilizes at 30.0 °C after a sharp downward trend within the first 2 min. It remains for most of the duration, apart from a slight disturbance at minute 20. This indicates that existence of a cooling fan helps maintain the FC thermal equilibrium slightly above the ambient temperature. Test 2 and Test 3 record a slightly higher ambient temperature at approximately 30.7 °C. Test 2, the temperature is consistently higher (around 31 °C) compared to Test 1, with very small fluctuations. A slight increase was observed at minute 27, in which it approaches 31.4 °C. This suggests that accumulation of heat due to continuous operation under similar conditions. Test 3, the temperature begins around 31.2 °C and slowly decreases to 30.8 °C immediately after the cooling fan is switched on at minute 6 (marked by the green line).

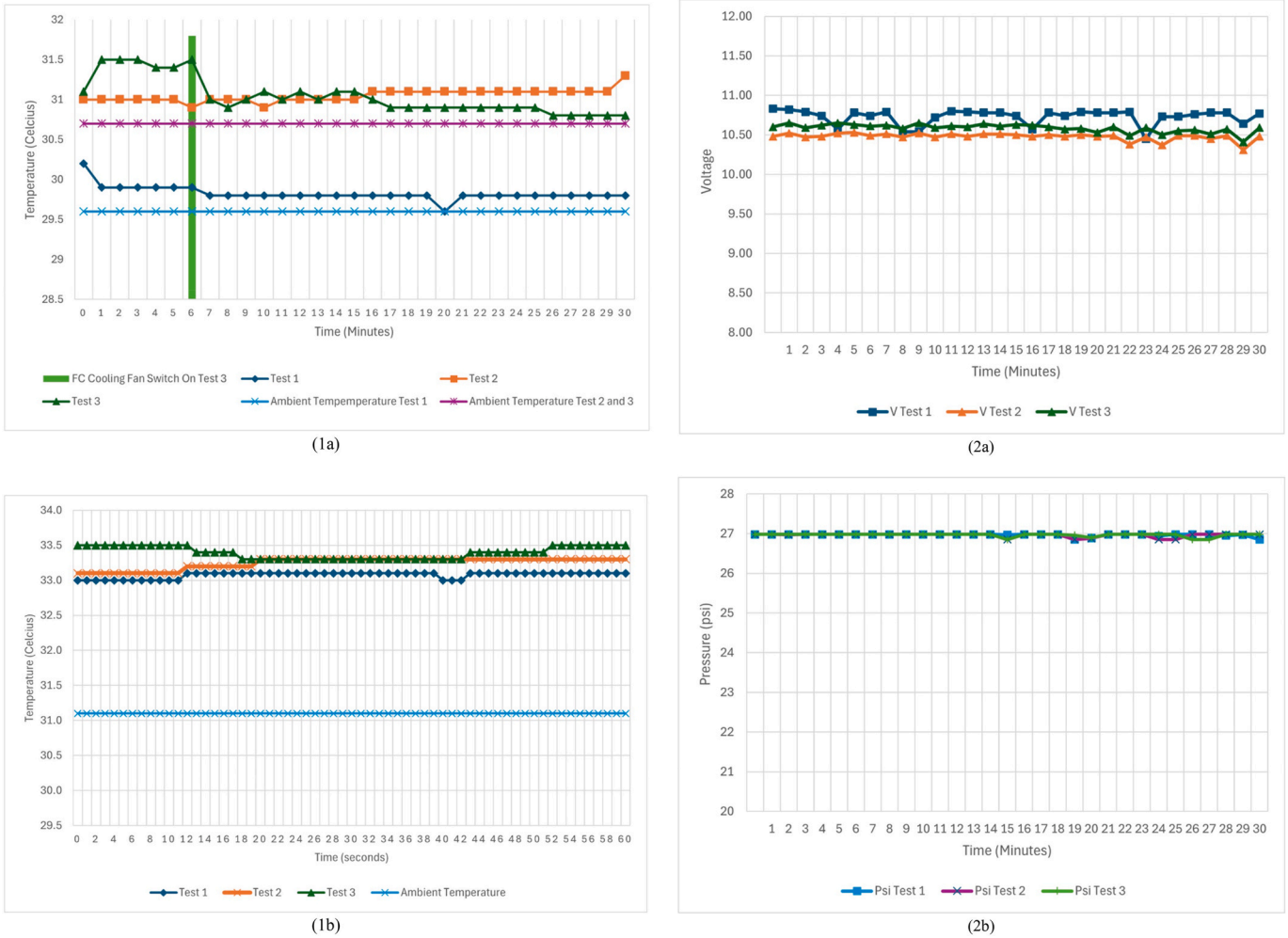

Fig. 6. Fuel Cell Performance (1a) Temperature of Fuel Cell (Without commercial Controller) Vs Time (1b) Temperature of Fuel Cell Connected with Controller (commercial) Vs Time (2a) Pressure Output (Without commercial FC Controller) Vs Time (2b) Fuel Cell Voltage Output (Without commercial FC Controller) Vs Time.

Thereafter, the temperature stabilizes and mirrors the same trend in Test 2, albeit with slightly lower values. This demonstrates the effect of forced convection cooling in reducing the thermal build-up of the FC.

Fig. 6(1b) demonstrates FC temperature (with the integration of a commercial controller) vs time across three independent tests: Test 1 (blue line), Test 2(orange line) and Test 3(dark green line). Across all tests, the measured temperature for the FC is around 33.5 °C. These tests were done concurrently with the results in Fig. 5(b) (refer Section 3.3.1). The only logical explanation for this type of setting is that there might be for controlling the temperature of the FC at an optimized level. Based on previous studies by Abdullah and Gan [32], Lochner et al. [33] and Zhou et al. [34], their findings do indicate that optimize temperature can improve efficiency but the temperature range for the optimize value can reach 120 °C [33] and up to 160 °C [34]. For the current study, the optimal operating external temperature is 55 °C [18]. So, the intermittent on-off settings are still something that needs to be studied. Fig. A4 is the operational sequence of the current fuel cell controller.

Fig. 6(2b) demonstrates the effect of three independent tests on pressure (Psi Test 1, Psi Test 2 and Psi Test 3) vs Time and Fig. 6(2a) FC voltage output Test 1 (V Test 1), FC voltage output Test 2 (V Test 2) and FC output Test 3 (V Test 3) vs Time. From the results of these three tests, the data confirms that pressure variations do not compromise voltage stability. Analyzing Fig. 6(2a) and (2b), the voltage for all tests is identical remaining steady at around 10.4 V. In addition, the pressure for Test 1, Test 2 and Test 3 stabilizes at around 27 psi (186.2 kPa). There were no fluctuations in the trend. This indicates that the electrolyzer has an inbuilt pressure control mechanism [18].

In conclusion, the changes in pressure and temperature did not affect the output of the FC. Based on the technical information of FC [18], the external operational temperature could reach 55 °C and output will still be constant.

3.3. *New fuel cell controller*

The FC controller is a critical component in ensuring stable and efficient system performance. It regulates the dynamic interaction between hydrogen supply, pressure, temperature, and electrical load demand [35,36]. In technical terms, the controller governs key operational parameters. These parameters in Fig. 5(b) are the activation of exhaust valve and stack voltage regulation, thereby preventing over-pressurization and voltage fluctuations. In addition, advanced controllers incorporate safety mechanisms and diagnostic algorithms that detect anomalies [35]. This will enhance protection of stack and downstream devices from accelerated degradation. On the contrary, inadequate control strategies lead to voltage instability and reduced stack lifetime, which ultimately compromise the reliability of the whole system. Thus, the FC controller is indispensable not only for maintaining operational stability but also ensuring safe integration with sensitive electronic load.

Supplementary Material, Figure B1(a) and (b) describe the pressure measured at the output of the hydrogen generator that is connected to the FC and on the hydrogen generator after the calibration conducted on

the pressure sensor. This comparison is essential to ensure the calibration readings from both pressure gauges and the pressure sensor are consistent. The reading for all pressure gauges and the pressure sensor peaked at around 26 psi or 185 kPa. The fixed reading can be concluded by the existence of the hydrogen generator pressure control system, which limits the system's pressure to not go above this predetermined pressure [18].

Fig. 7 presents the control experiments conducted on the newly implemented FC controller, comprising two independent tests, which were Test 1 and Test 2. Fig. 7(a) is defined as FC voltage output for test 1 (FC Volt T1) and test 2 (FC Volt T2). Fig. 7(b) is defined as pressure in psi for test 1 (Psi Test 1) and test 2 (Psi Test 2) and lastly Fig. 7(c) is defined as temperature in degrees Celsius for test 1 (T Test 1) and test 2 (T Test 2) respectively.

Test 1 measurements were taken during the initial startup of the hydrogen generator. The pressure exhibited a gradual increase until it stabilized at around 26.7 psi. During the pressure increase, the voltage output was unstable until the 15th minute, until it reached a stable voltage output of 10.5 V. The temperature of the FC was stable at around 31 °C throughout the test.

Test 2 was conducted under conditions where the electrolyzer was already operating at a stable pressure of 26.7 psi. The resulting voltage was stable at 10.5 V, which corresponds to the final stabilized data observed in Test 1. The temperature in test 2 is slightly higher at 32.5 °C, since the test was conducted an hour after test 1. It was conducted in such a way to observe the stability of readings from the new FC controller. The two tests demonstrate that the new FC controller can be employed for the current 30W FC or any other FC that would be utilized for future applications.

Figure B2 displays the voltage, temperature and system pressure of the new FC controller and exhaust valve conditions before the start-up of the hydrogen generator. The display can assist operators in monitoring

Table 5
Comparison of commercial FC controller against new FC controller.

Parameter	Commercial FC Controller	New FC Controller
Temperature Detection	×	/
Temperature Monitor	×	/
Voltage Detection	×	/
Voltage Control	/	/
Voltage Monitor	×	/
Pressure Detection	×	/
Pressure Control	/	/
Pressure Display	×	/
Smart Exhaust Valve Control	×	/
Power Supply	Fuel Cell	External power
Price (Malaysian Ringgit)	3700	200
Effected by Noise	Not tested	Effected

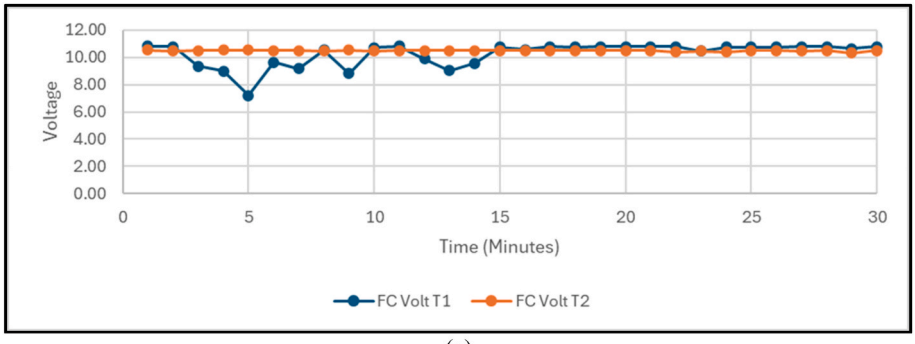

(a)

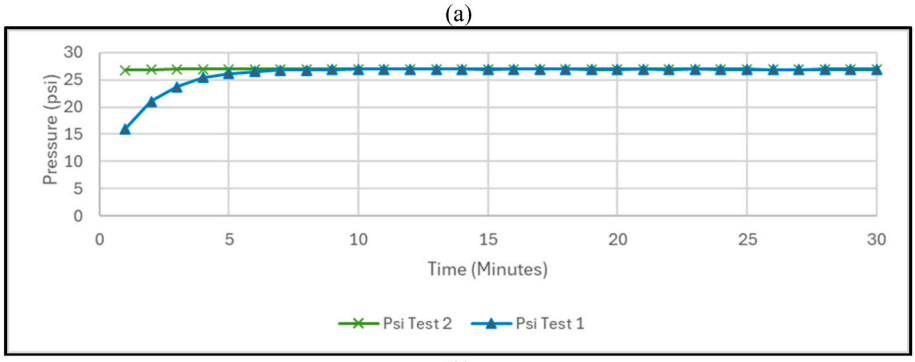

(b)

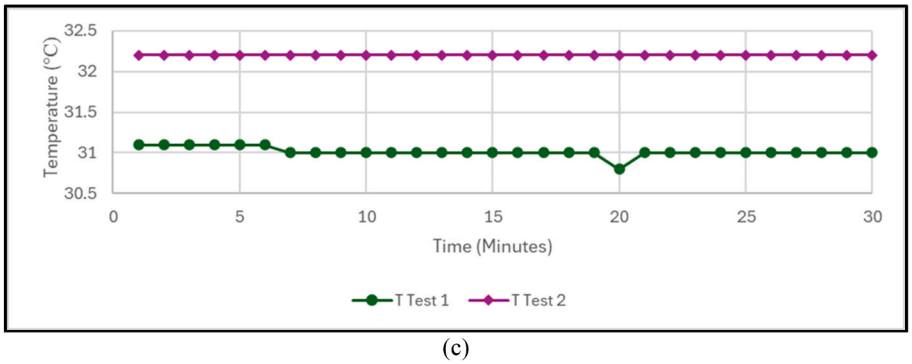

(c)

Fig. 7. Result of new fuel cell controller curve (a) FC voltage vs time (b) pressure vs time (c) temperature vs time.

the fuel cell and hydrogen generator more effectively.

Table 5 is the comparison parameters between the commercial FC controller and new FC controller. The table describes the advantages and limitations of each individual FC controller.

The new FC controller use a DS18B20 sensor for measuring temperature that has a range of −55 °C to +125 °C, providing a 9 to 12-bit resolution and ± 0.5 °C accuracy within a range of −10 °C to +85 °C. The new FC controller is set to activate a Red LED when the FC temperature is 40 °C. This is to alert the operator to inspect the FC for any damage to the cooling fan or maybe an external heat being added to the system.

For measuring voltage, a sensor with a 25V specification is used to measure FC voltage. The voltage detection range of the sensor is approximately 0.02445V to 25V. The FC output voltage needs to be 8.4V and above for a normal operating condition. A green LED will be activated when the voltage is 8.4V and above. This is to indicate the FC is in good condition.

Lastly, for pressure control and monitoring, a DC 5V 1/8 NPT pressure sensor is used. The sensor features a 0.5V to 4.5V linear output with a ± 2% full-scale accuracy, that has a wide operating temperature of −40 °C to +120 °C. The operating pressure of the commercial hydrogen generator is 400 kPa. Therefore, to maintain an optimal pressure-setting, an exhaust valve that activates when the pressure is 200 kPa will be activated, to relief the system's pressure to an optimal level.

All the measured parameters, i.e. temperature, voltage and pressure, are displayed using a 20x4 LCD for easy and efficient monitoring of the FC operating conditions and overall performance.

In summary, the new FC controller gives more advantages on the monitoring aspect of the dynamic changes in the voltage, temperature and pressure of the FC.

- Stabilization of Voltage through Adaptive Pressure Control. The transition from a commercial timer-based controller to our novel analog controller yielded a critical outcome: the stabilization of the PEM fuel cell's output voltage from fluctuations exceeding 7 V to a consistent 10.5 V. This improvement is not merely a performance metric but is indicative of resolving fundamental physicochemical challenges within the stack. The severe voltage fluctuations observed with the commercial controller are symptomatic of ineffective water management leading to mass transport limitations. In PEMFCs, particularly under conditions resembling dead-end operation, liquid water accumulation blocks reactant pathways to the catalyst sites—a condition known as reactant starvation, which directly causes voltage drops and instability [37,38]. The fixed-time purge cycle of the commercial unit fails to adapt to the dynamic rate of water production, likely creating alternating states of cathode flooding (causing voltage drops) and membrane dry-out. Our controller directly targets this root cause by implementing a pressure-triggered adaptive purge strategy. We utilize stack pressure as an integrative state variable for the internal gas/water balance. An increase in pressure toward our 200 kPa setpoint signals product accumulation. Triggering the exhaust valve at this threshold provides a purge responsive to the actual system state, thereby maintaining clear mass transport pathways and preventing the reactant starvation that leads to voltage undershoots [38].
- Implementation of the Control System. To execute this strategy, the controller integrates specific sensors for monitoring and control. A DS18B20 sensor (±0.5 °C accuracy) monitors stack temperature, with a visual alert at 40 °C to flag cooling issues. Voltage is tracked via a 25V-range sensor, with a green LED indicating healthy operation above 8.4V. Crucially, a 5V pressure sensor (1/8 NPT, ±2% accuracy) provides the input for the core control logic: activating an exhaust valve at 200 kPa to regulate system pressure. All parameters are displayed on a 20x4 LCD for operational monitoring.
- Implications for System Durability and Accessibility. The controller's ability to maintain voltage stability has direct implications for system efficiency and durability. Conditions that cause voltage instability, such as repeated reactant starvation, are known to promote catalyst layer corrosion and accelerate membrane degradation, severely impacting the system's operational lifespan [39]. Therefore, our controller contributes to prolonged operational reliability. A significant ancillary outcome is the drastic cost reduction to under MYR 200 (approximately 18 times less than the commercial unit), making such responsive control accessible for research and small-scale applications.

One obvious limitation the new FC controller can be observed is the effect of noise on its reading. Shielding electronic components should also be studied to reduce or even cancel noise indefinitely. Further improvements can be achieved for the new FC controller by incorporating additional monitoring modules or implementing suitable control methods, such as repetitive control [40] if deemed applicable for the improvement of the controller's reliability and diagnostic capability.

4. Conclusions

This study successfully developed an affordable new FC controller and established the following key findings:

The Hydrogen Generator GL200 exhibits a stable production output of 210 ml/min with the system pressure maintained at 27 psi or 185 kPa under the blocked-output conditions. The operational parameters are regulated and monitored by the system pressure controller. The hydrogen generator operates with a power of less than 100W, in which the estimated efficiency of the hydrogen generator for hydrogen production ranging between 33.7% and 42.7%.

The commercial FC controller have a few advantages. It is capable to use the power produce from the 30W FC and regulating the voltage output. Experimental results indicate an observable voltage increase of approximately 1.2 V. The exhaust valve is activated at a preset-repeating cycle, specifically at the 5th second, to maintain the system's pressure at optimal range. At the 10th second, the FC output is cut off, in which at certain occurrences, a voltage drop of 7 V can be observed. This operating condition can likely reduce the life cycle of electrical components or devices in the long run. The other weaknesses that can be observed from the investigations are the controller lacks integrated pressure, temperature and voltage sensors which are essential for more optimal monitoring. The most critical issue is the cost, as the controller is valued at Malaysian Ringgit 3700 for a relatively simple functionality.

The new developed FC controller is identified as Automated Voltage-Temperature Monitoring and Pressure-Based Valve Control System using Analog Voltage Input. The new FC controller incorporates an LCD display for effective and easy monitoring. In addition, it is also equipped with voltage, pressure and temperature sensors to detect any dynamic changes in the system's pressure, FC voltage output and FC temperature. The exhaust valve is programmed to activate when the system's pressure is at 200 kPa. This will protect the system from overpressure. Furthermore, the new FC controller has a stable output of around 10.5V to 10.7 V, slightly lower than the commercial FC controller. A key advantage of our prototype is its significantly lower cost; at approximately RM 200, the controller is around 18 times more affordable than existing solutions. This cost-effective approach introduces inherent engineering challenges, such as susceptibility to environmental noise; however, these are well-understood and already have clear solutions in development. Our immediate future work will prioritize implementing robust filtering algorithms to mitigate noise and deliver higher measurement precision. Next, we will integrate additional monitoring modules to enhance diagnostic capabilities and overall reliability. Concurrently, we will investigate advanced shielding techniques to permanently minimize interference.

CRediT authorship contribution statement

Ephrem Ryan Alphonsus: Writing – original draft, Methodology, Investigation, Data curation. **Mohammad Omar Abdullah:** Writing – review & editing, Supervision, Methodology, Funding acquisition, Conceptualization. **Ahmed M.A. Haidar:** Writing – review & editing, Supervision. **Abadi Chanik:** Validation. **Ibrahim Yakub:** Validation. **Thossaporn Wijakmatee:** Writing – review & editing, Validation. **Hideyuki Matsumoto:** Writing – review & editing.

Declaration of generative AI and AI-assisted technologies in the writing process

During the preparation of this work the author(s) used ChatGPT to improve language and readability. After using this tool/service, the author(s) reviewed and edited the content as needed and take(s) full responsibility for the content of the publication.

Declaration of competing interest

The authors declare that they have no known competing financial interests or personal relationships that could have appeared to influence the work reported in this paper.

Acknowledgements

This work was supported by the VC High Impact Research Grant 2.0 (VC HIRG2.0), UNIMAS, Sarawak, Malaysia, under Grant No: UNI/F02/VC-HIRG-2/86108/2023. under Grant No: UNI/F02/VC-HIRG-2/86108/2023. The first author, Ephrem Ryan Alphonsus, was the recipient of a PhD scholarship from this grant. The authors also thank UNIMAS for its ongoing institutional support. Furthermore, the authors gratefully acknowledge the collaborative support provided by the Institute of Science Tokyo.

Appendix A. Supplementary data

Supplementary data to this article can be found online at https://doi.org/10.1016/j.ijhydene.2026.154311.

Data availability

Data available on request from the Authors.

References

[1] Hren R, Vujanović A, Van Fan Y, Klemeš JJ, Krajnc D, Čuček L. Hydrogen production, storage and transport for renewable energy and chemicals: an environmental footprint assessment. Renew Sustain Energy Rev 2023;173. https://doi.org/10.1016/j.rser.2022.113113.

[2] Abdelhamid HN. A review on hydrogen generation from the hydrolysis of sodium borohydride. Int J Hydrogen Energy 2021;46(1):726–65. https://doi.org/10.1016/j.ijhydene.2020.09.186. Elsevier Ltd.

[3] Hassan NS, Jalil AA, Rajendran S, Khusnun NF, Bahari MB, Johari A, Kamaruddin MJ, Ismail M. Recent review and evaluation of green hydrogen production via water electrolysis for a sustainable and clean energy society. Int J Hydrogen Energy 2024;52:420–41. https://doi.org/10.1016/j.ijhydene.2023.09.068.

[4] Martinez-Burgos WJ, de Souza Candeo E, Pedroni Medeiros AB, Cesar de Carvalho J, Oliveira de Andrade Tanobe V, Soccol CR, Sydney EB. Hydrogen: current advances and patented technologies of its renewable production. J Clean Prod 2021;286. https://doi.org/10.1016/j.jclepro.2020.124970. Elsevier Ltd.

[5] Al Dhahri H, Hussain M, Ghani MAA, Inayat A, Al-Muhtaseb AH, Al-Haj L, Jamil F. Green hydrogen production via electrolysis: materials innovation, system integration, and global deployment pathways. In: Renewable and sustainable energy reviews, 29. Elsevier Ltd; 2026. https://doi.org/10.1016/j.rser.2025.116617.

[6] Nikolaidis P, Poullikkas A. A comparative overview of hydrogen production processes. Renew Sustain Energy Rev 2017;67:597–611. https://doi.org/10.1016/j.rser.2016.09.044. Elsevier Ltd.

[7] Dawood F, Anda M, Shafiullah GM. Hydrogen production for energy: an overview. Int J Hydrogen Energy 2020;45(7):3847–69. https://doi.org/10.1016/j.ijhydene.2019.12.059. Elsevier Ltd.

[8] Harrison K, Ivy Levene J. Electrolysis of water. In: Rajeshwar K, McConnell R, Licht S, editors. Solar hydrogen generation: toward a renewable energy future. 2008 Edition. Springer; 2008. p. 41–63. https://doi.org/10.1007/978-0-387-72810-0_3.

[9] Liu Y, Akundi SS, Braniff A, Dantas B, Niknezhad SS, Tian Y, Khan F, Pistikopoulos EN. Process monitoring and safety-informed control of a proton exchange membrane water electrolysis system. AIChE J 2025;71(9). https://doi.org/10.1002/aic.18909.

[10] Bakır H, Ağbulut Ü. Efficient design, operation and control of commercial proton exchange membrane fuel cells (PEMFCs) in clean energy technology. Int J Hydrogen Energy 2026;197. https://doi.org/10.1016/j.ijhydene.2025.152498.

[11] Qi W, Yu L, Tang X, Wu J, Zhang Y, He Z. Multi-objective optimization of a hydrogen-fueled PEMFC with multi wavy channels via machine learning and CFD simulation. Int J Hydrogen Energy 2026;199:152748. https://doi.org/10.1016/j.ijhydene.2025.152748.

[12] Fang S, Feng J, Zhu Y, Chen Z, Fang X, Chen D, Fan X. Coordinated optimization and management of oxygen content and cathode pressure for PEMFC based on hybrid nonlinear robust control. Science and Technology for Energy Transition 2025;80:5. https://doi.org/10.2516/stet/2024098.

[13] Li Y, Zheng Z, Guo Y, Cheng X, Yan X, Wei G, Shen S, Zhang J. Control-oriented thermal management strategies for large-load fluctuation PEM fuel cell systems. Appl Energy 2025;392:125915. https://doi.org/10.1016/j.apenergy.2025.125915.

[14] Fan S, Xu S. Optimal fuel cell control modeling with feedback linearization and adaptive sliding mode control. Sci Rep 2026. https://doi.org/10.1038/s41598-026-35888-6.

[15] LNI Swissgas. (n.d.). HG kube V2. https://Www.Lni-Swissgas.Eu/En/Product/Hg-Kube-V2/.

[16] PEAK Scientific. (n.d.). Hydrogen gas generators. https://Www.Peakscientific.Com/Products/Hydrogen/.

[17] Parker Hannifin Corporation. (n.d.). Hydrogen generators for gc combustion detector application. https://Ph.Parker.Com/My/En/Product-List/Hydrogen-Generators-for-Gc-Combustion-Dectector-Applications.

[18] Shandong Saikesaisi Hydrogen Energy Co., Ltd. (n.d.). Operation manual for QL hydrogen generators.

[19] Tianjin Hyvoda Hydrogen Energy Technology Co., Ltd. (n.d.). China ultra pure hydrogen generator with PEM electrolysis 9N. made-in-China.com. https://Hyvoda.En.Made-in-China.Com/Product/BdpGNislSXaZ/China-Ultra-Pure-Hydrogen-Generator-with-Pem-Electrolysis.

[20] Honsho Y, Nagayama M, Matsuda J, Ito K, Sasaki K, Hayashi A. Durability of PEM water electrolyzer against wind power voltage fluctuation. J Power Sources 2023;564:232826.

[21] Bareiß K, de la Rua C, Möckl M, Hamacher T. Life cycle assessment of hydrogen from proton exchange membrane water electrolysis in future energy systems. Appl Energy 2019;237:862–72. https://doi.org/10.1016/j.apenergy.2019.01.001.

[22] Anwar S, Khan F, Zhang Y, Djire A. Recent development in electrocatalysts for hydrogen production through water electrolysis. Int J Hydrogen Energy 2021;46(63):32284–317. https://doi.org/10.1016/j.ijhydene.2021.06.191.

[23] Chisholm G, Cronin L. Hydrogen from water electrolysis. In: Storing energy: with special reference to renewable energy sources. Elsevier Inc; 2016. p. 315–43. https://doi.org/10.1016/B978-0-12-803440-8.00016-6.

[24] Zhu Z, Weng Z, Zheng H. Optimal operation of a microgrid with hydrogen storage based on deep reinforcement learning. Electronics (Switzerland) 2022;11(2). https://doi.org/10.3390/electronics11020196.

[25] Mohamed B, Ali B, Ahmed B, Ahmed B, Salah L, Rachid D. Study of hydrogen production by solar energy as tool of storing and utilization renewable energy for the desert areas. Int J Hydrogen Energy 2016;41(45):20788–806. https://doi.org/10.1016/j.ijhydene.2016.07.034.

[26] Yunez-Cano A, González-Huerta R de G, Tufiño-Velázquez M, Barbosa R, Escobar B. Solar-hydrogen hybrid system integrated to a sustainable house in Mexico. Int J Hydrogen Energy 2016;41(43):19539–45. https://doi.org/10.1016/j.ijhydene.2016.06.203.

[27] Zainal BS, Ker PJ, Mohamed H, Ong HC, Fattah IMR, Rahman SMA, Nghiem LD, Mahlia TMI. Recent advancement and assessment of green hydrogen production technologies. Renew Sustain Energy Rev 2024;189(Part A). https://doi.org/10.1016/j.rser.2023.113941.

[28] Liu XW, Plumbridge WJ. Thermomechanical fatigue of Sn-37 wt.% Pb model solder joints. Mater Sci Eng, A 2003;362(1–2):309–21. https://doi.org/10.1016/S0921-5093(03)00638-5.

[29] Yang G, Meng K, Deng Q, Chen W, Xia W, Li Q, Chen B. Experimental investigation on operational stability and its influencing mechanisms for PEMFC with dead-ended anode. Int J Hydrogen Energy 2024;87:539–53.

[30] Valverde L, Rosa F, Bordons C, Guerra J. Energy management strategies in hydrogen smart-grids: a laboratory experience. Int J Hydrogen Energy 2016;41(31):13715–25. https://doi.org/10.1016/j.ijhydene.2016.05.279.

[31] Abe JO, Popoola API, Ajenifuja E, Popoola OM. Hydrogen energy, economy and storage: review and recommendation. Int J Hydrogen Energy 2019;44(29):15072–86. https://doi.org/10.1016/j.ijhydene.2019.04.068. Elsevier Ltd.

[32] Abdullah MO, Gan YK. Feasibility study of a mini fuel cell to detect interference from a cellular phone. J Power Sources 2006;155(2). 331–318.

[33] Lochner T, Kluge RM, Fichtner J, El-Sayed HA, Garlyyev B, Bandarenka AS. Temperature effects in polymer electrolyte membrane fuel cells. Chemelectrochem 2020;7(17):3545–68. https://doi.org/10.1002/celc.202000588. Wiley-VCH Verlag.

[34] Zhou M, Frensch S, Liso V, Li N, Sahlin SL, Cinti G, Simon Araya S. Modeling the performance degradation of a high-temperature PEM fuel cell. Energies 2022;15 (15). https://doi.org/10.3390/en15155651.
[35] Daud WRW, Rosli RE, Majlan EH, Hamid SAA, Mohamed R, Husaini T. PEM fuel cell system control: a review. Renew Energy 2017;113:620–38. https://doi.org/10.1016/j.renene.2017.06.027. Elsevier Ltd.
[36] Swain P, Jena D. 2015 international conference on recent developments in control, automation and power engineering. 2015.
[37] He P, Zhang Q, Mu Y, Qu Z, Yin J, Li Z, Chen J, Tao WQ. Temperature-dependent cathode starvation effects on cold start behavior of PEMFC stacks: an experimental investigation. Appl Energy 2026;406. https://doi.org/10.1016/j.apenergy.2025.127299.
[38] Liu Y, Zhao J, Tu Z, Hwa Chan S. Optimization strategies to mitigate reactant starvation in a dead-ended hydrogen–oxygen proton exchange membrane fuel cell during cyclic loading. Fuel 2024;357. https://doi.org/10.1016/j.fuel.2023.129886.
[39] Seselj N, Cleemann LN, Torres T, Azizi K. Advancing HT-PEM fuel cell technology: durability and performance under start–stop conditions. J Mater Chem A 2025;13 (47):40500–36. https://doi.org/10.1039/D5TA07002C.
[40] İnci M, Çelik Ö. Repetitive control strategy for grid integration of vehicular fuel cells to enhance system stability and robustness. J Power Sources 2025;642. https://doi.org/10.1016/j.jpowsour.2025.236992.